ACS APPLIED MATERIALS & INTERFACES

Research Article

www.acsami.org

Self-Assembled Monolayers of C_{60}–Triphenylamine Dyads as Photo-Switched Interfacial Layers for Potential Application in Photovoltaic Cells

Mahsa Hosseini,[‡] Danisha M. Rivera-Nazario,[‡] and Luis A. Echegoyen*

Department of Chemistry, University of Texas at El Paso, 500 W. University Avenue, El Paso, Texas 79968, United States

Supporting Information

ABSTRACT: C_{60}–Triphenylamine dyads were synthesized for incorporation as photoswitched interfacial layers in organic photovoltaic (OPV) cells. Self-assembled monolayers (SAMs) of these dyads on gold (through S–Au and C_{60}–Au interactions) were prepared through one or two adsorption processes, and their packing densities were fully characterized. Analysis using quartz crystal microbalance (QCM) and electrochemical impedance spectroscopy (EIS) measurements indicated that all SAMs exhibit dense coverage on the gold surfaces. Electrochemical desorption in KOH confirmed that the *cis*-**1** dyad is anchored to the gold surface through its thiol group. Impedance measurements in the absence and presence of UV irradiation were performed to observe the photoswitched properties of these surface confined dyads. Upon UV light exposure of the SAMs, the charge-transfer resistance decreased when $Fe(CN)_6^{3-/4-}$ was used as the probe redox couple and increased with $Ru(NH_3)_6^{3+/2+}$, confirming the generation of positive charges on the surface upon UV irradiation.

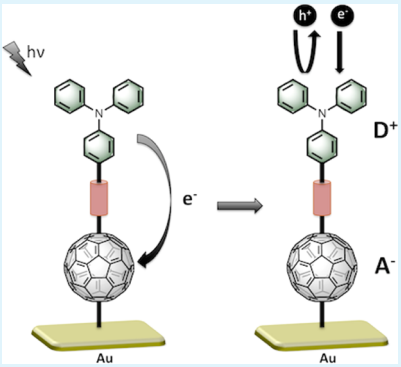

KEYWORDS: *fullerene-based dyad, self-assembled monolayer, interfacial layer, organic photovoltaic cell, electrochemical impedance*

1. INTRODUCTION

Organic photovoltaic (OPV) devices, while not as efficient energy-wise as inorganic ones, are considered to be of great potential for cost efficient solar cell technology because of their electronic and optical properties, their light weight, and their mechanical flexibility.[1−4] A requirement for higher efficiency is the proper collection of charge carriers while minimizing charge recombination processes.[5−8] To accomplish this, it is important to collect the majority of the charge carriers while blocking the counterparts to create a depletion region to improve the diffusion and to polarize the OPV device to increase drift velocities.[6−9] A variety of interfacial treatments and materials has been used to improve the charge transport/blocking and the ohmic contacts at both cathode/organic and anode/organic interfaces.[10,11] Poly(3,4-ethylenedioxythiphene):poly-(styrenesulfonate) (PEDOT:PSS) has been widely used as an interfacial layer (IFL) which exhibits good hole transport in contact with tin-doped indium oxide (ITO) in typical OPV anodes. However, the inhomogeneity of the electrode surface results in some limiting factors for stability and performance of OPVs, such as high series resistances, acidity, and low durability caused by degradation under UV illumination.[12,13] It has been reported that self-assembled monolayers (SAMs) in OPVs can block currents at the cathode or serve as moisture blocking layers and as dipolar surface layers to enhance charge injection.[14−16] Moreover, it has been shown that the use of a polarized SAM as an IFL can increase the photoconversion efficiency of small-molecule OPV devices.[17] On the basis of these reports, electrical polarization at interfacial layers in anodes or cathodes should increase the efficiency of OPV devices. Using donor–acceptor (D–A) dyads with the correct molecular orientation should lead to D^+–A^- charge separated states upon photoexcitation and in turn to enhanced OPV device efficiencies. Light-induced charge separation plays an important role in the design of OPVs based on D–A systems. Several investigations have shown that the lifetimes of the charge-separated states (D^+–A^-) can be controlled by different parameters such as: the nature of the D–A[18] spacer (linker) between the donor and acceptor[19−21] and the length and orientation of the spacer.[22,23] C_{60} has been used widely as an electron acceptor in D–A dyad systems due to its unique three-dimensional structure, low reorganization energy upon reduction, and good electron accepting properties.[19−25] Among the many electron donor molecules that have been used,[26−28] triphenylamine (TPA) is known as a relatively strong light absorber and it has excellent hole transporting properties.[25,29,30] In this work, we focused on the design, syntheses, and analyses of D–A dyad (TPA–C_{60}) SAMs as IFLs in which the acceptor (C_{60}) is attached (adsorbed) to the anode (gold) by an anchoring group (Figure 1). Upon illumination, the TPA–C_{60} dyads form charge-separated states that should function as hole-blocking/electron transporting (HB/ET) layers. Electrochemical impedance spectroscopy was employed to investigate the surface properties of the SAMs

Received: January 3, 2014
Accepted: February 13, 2014
Published: February 13, 2014

   dx.doi.org/10.1021/am500049q | ACS Appl. Mater. Interfaces 2014, 6, 3712−3720

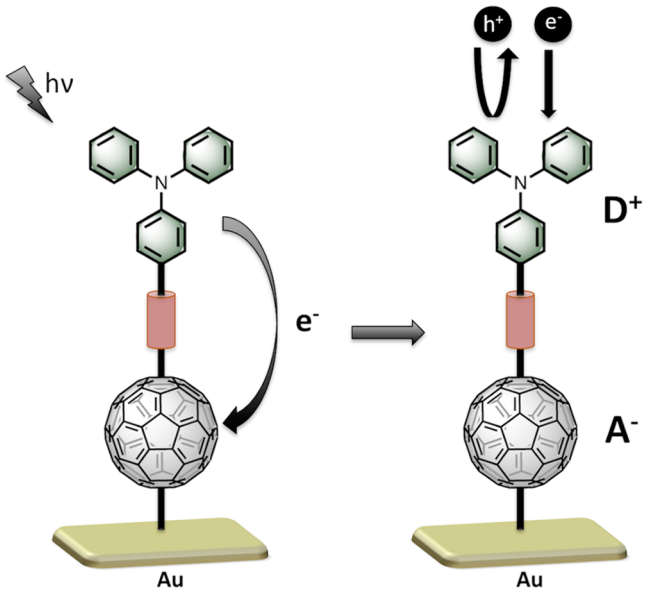

Figure 1. Concept of photoswitched donor−acceptor (D^+−A^-) SAM on a gold surface.

using both a negative as well as a positive electrochemical probe. Three SAMs containing TPA−C_{60} dyads with different linkers were prepared and their optical, physical, and chemical properties were investigated using different techniques.

2. EXPERIMENTAL SECTION

2.1. Synthesis of Photoswitched Fullerene-Based Dyads *trans*-1 and *cis*-1. Anhydrous chlorobenzene was purchased from Sigma-Aldrich and used as received. 4-(Diphenylamino)benzaldehyde was purchased from Aldrich, and DL-homocysteine was purchased from TCI America; both were used as received. C_{60} 99.5+% was purchased from SES Research and used as received. ^{1}H and ^{13}C NMR spectra were recorded on a JEOL ECA 600 NMR spectrometer at room temperature using $CDCl_3$ or $CDCl_3$:CS_2 as solvent. UV-vis spectra were collected at room temperature using a Varian UV-vis-NIR Cary 5000 spectrophotometer. Mass spectra were obtained using a Bruker microFlex MALDI-TOF spectrometer on reflector positive mode using 1,8,9-trihydroxyanthracene as the matrix.

2.1.1. Synthesis of mono-2-(ethanethiol)-5-((4-diphenylamino)-phenyl)fulleropyrrolidine (trans-1 and cis-1). Note: this nomenclature should not be confused with C_{60} *bis*-adduct nomenclature. The general procedure for 1,3-dipolar cycloaddition reactions was followed.[31] C_{60} (100 mg, 0.14 mmol) was added to a 100 mL Schlenk flask along with 4-(diphenylamino)benzaldehyde (17 mg, 0.07 mmol) and DL-homocysteine (47 mg, 0.35 mmol). The mixture was dissolved in 50 mL of anhydrous chlorobenzene and heated to 150 °C under Argon for 12 h. After 12 h, the reaction mixture was allowed to cool down and the solvent was finally removed under reduced pressure. The remaining solid was then dissolved in CS_2 and chromatographed using a silica gel column, eluting first with CS_2 to remove the unreacted C_{60} followed by toluene to elute two fractions of diastereomers (*trans*-**1**, 2.0 mg, 3% yield; *cis*-**1**, 16.8 mg, 22% yield). Note: *cis*-**1** was used for SAM formation and analysis.

trans-**1**. R_f = 0.48 (silica gel, toluene); ^{1}H NMR (600 MHz, $CDCl_3$) δ (ppm): 7.58 (d, J = 8.6 Hz, 2H), 7.24−7.19 (m, 4H), 7.12 (d, J = 8.5 Hz, 2H), 7.04 (d, J = 8.9 Hz, 3H), 7.01 (t, J = 7.5 Hz, 3H), 5.95 (s, 1H), 5.36 (dd, J = 11.5, 3.9 Hz, 1H), 3.28−3.18 (m, 2H), 3.18−3.09 (m, 1H), 3.09−3.01 (m, 1H), 2.68−2.61 (m, 1H), 1.73 (t, J = 8.0 Hz, 1H). UV−vis λ_{max} (nm): 309, 431; Anal. Calcd for $C_{82}H_{22}N_2S$: C, 92.29; H, 2.08; N, 2.63; S, 3.00. Found: C, 91.13; H, 2.02; N, 2.61; S, 3.12.

cis-**1**. R_f = 0.39 (silica gel, toluene); ^{1}H NMR (600 MHz, $CDCl_3$) δ (ppm): 7.63 (d, J = 8.7 Hz, 2H), 7.22−7.18 (m, 4H), 7.08 (d, J = 8.7 Hz, 2H), 6.99 (dd, J = 15.7, 7.6 Hz, 6H), 5.79 (s, 1H), 5.01 (dd, J = 10.4, 2.7 Hz, 1H), 3.25−2.98 (m, 4H), 2.69−2.61 (m, 1H), 1.70 (t, J = 8.0 Hz, 1H); ^{13}C NMR (151 MHz, $CDCl_3$:CS_2) δ (ppm): 153.60, 153.45, 153.26, 152.96, 147.90, 147.31, 147.12, 147.09, 146.65, 146.43, 146.30, 146.20, 146.19, 146.18, 146.14, 146.02, 145.94, 145.88, 145.86, 145.60, 145.48, 145.37, 145.32, 145.29, 145.14, 145.10, 144.60, 144.49, 144.31, 144.23, 143.17, 142.99, 142.68, 142.65, 142.60, 142.47, 142.32, 142.18, 142.10, 142.02, 141.99, 141.86, 141.65, 141.61, 140.13, 140.02, 139.67, 139.41, 137.00, 136.25, 136.06, 135.67, 130.76, 129.31, 129.07, 124.41, 123.40, 123.11, 78.79, 77.16, 76.28, 75.79, 70.56, 37.44, 23.81; UV−vis λ_{max} (nm): 308, 430; MALDI-TOF MS: calcd. 1067.16 [M + H]$^+$, found 1067.17 [M + H]$^+$. Anal. Calcd for $C_{82}H_{22}N_2S$: C, 92.29; H, 2.08; N, 2.63; S, 3.00. Found: C, 91.44; H, 2.04; N, 2.50; S, 3.01.

2.2. Preparation of Self-Assembled Monolayers on Au Surfaces. Gold on silicon substrates with a thickness of 100 nm Au over chromium were purchased from Sigma-Aldrich. Substrates were cleaned prior to SAM formation using sonication with DI water, isopropanol, and acetone, 15 min each. After drying with a flow of N_2 gas, the substrates were left under vacuum for 1 h at 50 °C. The cleaned Au electrodes were immersed for 48 h in a 4 mM ethanol/toluene (1:3) solution of the desire dyad, unless stated otherwise. The substrates were rinsed with ethanol and toluene to remove nonadsorbed molecules from the surface and dried under a nitrogen gas flow and then stored under vacuum at 50 °C before electrochemical measurements. Quartz crystal microbalance (QCM) measurements were used to determine the coverage extent and the amount of material deposited on the surface of the gold-coated quartz crystals. A QCM200 Digital Controller and QCM25 5 MHz Crystal Oscillator from Stanford Research Systems (SRS) were used. Five MHz, 1 in. diameter, AT-cut quartz crystal wafers (Cr/Au) with circular electrodes on both sides were purchased from SRS. The gold-coated crystals were sonicated in DI water, isopropanol, and acetone for 5 min each and dried with N_2 gas before use. Liquid immersion was the selected technique for the measurements. A crystal holder containing a clean gold-coated quartz crystal was immersed in a jacketed beaker containing anhydrous toluene. The temperature was kept at 25.0 ± 0.1 °C during all experiments. A baseline in pure toluene was established before adding the corresponding compounds.

2.3. Electrochemical Measurements. All electrolyte solutions for electrochemical measurements were prepared with DI water and purged with Ar before measurements were made unless stated otherwise. Electrochemical impedance spectroscopy (EIS) and cyclic voltammetric (CV) measurements were conducted using a three-electrode configuration at room temperature. A coiled platinum mesh, a $Ag/AgNO_3$ nonaqueous electrode separated by a vycor tip, and a modified gold substrate were used as counter, reference, and working electrodes, respectively, unless stated otherwise. All redox potentials were referenced to the Ag/Ag^+ electrode or to the redox couple of internally added Fc/Fc^+. Electrochemical experiments were performed with a CHI-660A electrochemical workstation. Impedance measurements were performed in a 0.1 M $NaPF_6$ solution containing equal concentrations of $Ru(NH_3)_6^{2+/3+}$ and $Fe(CN)_6^{3-/4-}$ (~1 mM). The frequency range used was 10^4 to 0.1 Hz with an AC amplitude of 5 mV. EIS data were analyzed by the Equivalent Circuit Simulation program included in the CHI-660A software package. A QCM Entela UVGL-58 Hand-held UV lamp (254/365 nm/6 W/0.12 Amps) was used for UV illumination at 365 nm. The electrochemical desorption experiments were conducted in a 0.5 M KOH solution purged with Ar for 25 min.

2.4. Contact Angle Measurements. The contact angles of water were measured using a Ramé-Hart model 250 goniometer using pure deionized water at room temperature with a relative humidity at a constant volume of 5 μL. A total of ten static measurements were analyzed and averaged for each self-assembled monolayer.

3. RESULTS AND DISCUSSION

3.1. Synthesis of TPA−C_{60}−thiol. The one-step synthetic procedure for the preparation of the thiol functionalized TPA−C_{60} dyad **1** is presented in Scheme 1. Treatment of C_{60} in

Scheme 1. Synthesis of Fullerene-Based Dyad 1

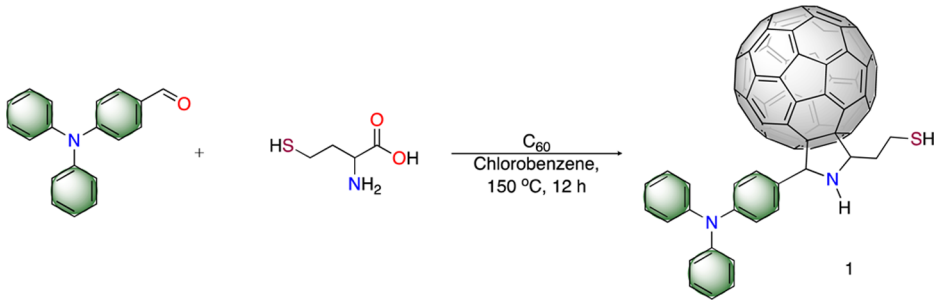

chlorobenzene with DL-homocysteine and 4-(diphenylamino)-benzaldehyde afforded a mixture of diastereomers: *trans*-**1** and *cis*-**1** (this nomenclature should not be confused with the nomenclature used for C_{60} *bis*-adduct). The compounds were characterized by ^{1}H NMR, ^{13}C NMR, COSY, NOESY, MALDI-TOF MS, cyclic voltammetry, and UV−vis (Figures S2−S12, Supporting Information). Although four diastereomers are possible (see Figure S1, Supporting Information), based on NOESY NMR experiments (Figures S3−S4 and S7−S8, Supporting Information), *trans*- and *cis*-structures were assigned, but not specific enantiomers. The synthesis of TPA−C_{60} dyad **2** (Figure S1, Supporting Information) was performed following the procedure previously reported by Pinzón et al.[32] Dyad **1** is a newly synthesized dyad, but conceptually similar ones reported in the literature could in principle work in a similar fashion.[20,21,33−35]

3.2. Preparation of SAMs on Au Surfaces. The general procedure for the preparation of the self-assembled monolayers was described in Section 2.2. A pictorial representation of the modified Au substrate with *cis*-**1** is depicted in Figure 2a, as **SAM 1**. The same procedure was followed to form a SAM of dyad **2** on the surface of Au, **SAM 2** (Figure 2b). The Mirkin group used a similar process to form a fullerene SAM on a Au surface.[36] For the preparation of TPA−C_{60}, **SAM 3**, two steps were required (Figure 2c). In the first step, the clean Au substrate was soaked in a 4 mM ethanolic solution of 4-aminothiophene for 3 days in order to ensure the formation of a densely packed monolayer (**SAM 3a**). This modified substrate was rinsed with ethanol and dried under a nitrogen flow followed by vacuum drying. In the second step, the substrate with **SAM 3a** was soaked in a 4 mM toluene solution of dyad **2** for 3 days, while refluxing under N_2.[37] The Au modified electrode was then rinsed and dried as described in Section 2.2 (**SAM 3b**).

3.3. Characterizations. *3.3.1. C_{60}-Based Dyads trans-1 and cis-1.* *trans*-**1** and *cis*-**1** were characterized by cyclic voltammetry (Figures S11 and S12, Supporting Information). The cyclic voltammogram of *cis*-**1** in 0.1 M of $TBAPF_6/CH_2Cl_2$ solution at a scan rate of 100 mV/s shows three reversible reduction peaks at −1.18, −1.57, and −2.07 V referenced to the redox couple Fc/Fc^+, corresponding to the reduction of the fullerene, and three irreversible oxidations at +0.47, +0.62, and +0.85 V corresponding to the −SH group, retro-cycloaddition,[38] and the TPA group, respectively. Although we are not certain, we assign the peak at +0.47 V to the oxidation of the −SH group. On the basis of the work of Han et al.,[39] it is difficult to detect cysteine oxidation using bare GC electrodes, but the presence of C_{60} has been shown to improve its detection,[40] so we tentatively assign the +0.47 V oxidation peak to the −SH group.

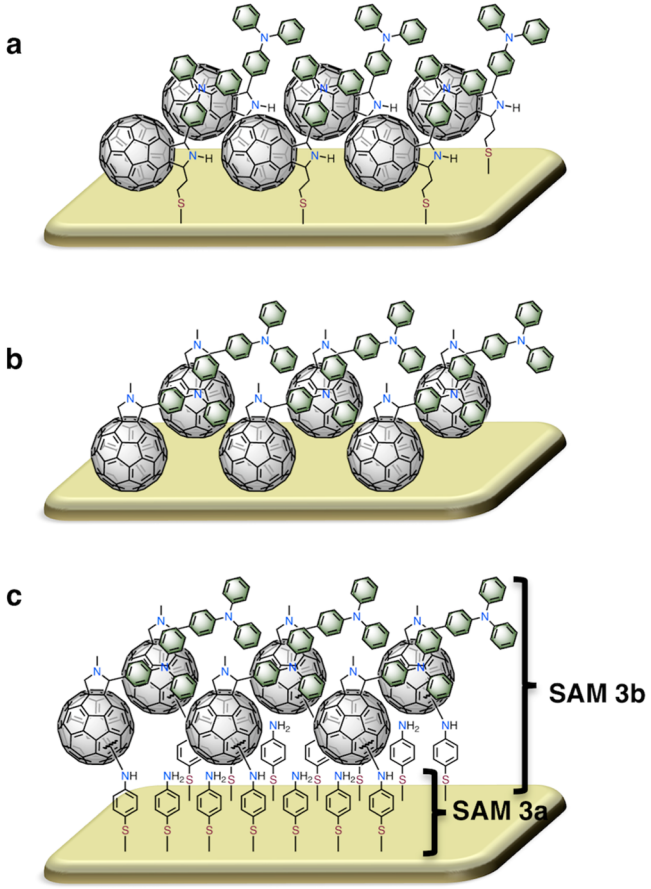

Figure 2. Pictorial representation of (a) **SAM 1**, (b) **SAM 2,** and (c) **SAM 3a** and **3b** on Au surface.

3.3.2. Self-Assembled Monolayers. Contact angle measurements are often used to study the wetting properties of a surface to reflect its hydrophobicity.[41] Self-assembled monolayers of organic materials at a surface decrease wettability while lowering the surface free energy. Table 1 shows the water

Table 1. Water Contact Angle Measurements before and after Monolayer Treatment

substrate	water contact angle (deg)
clean Au	62.94 ± 0.16
SAM 1	96.76 ± 0.17
SAM 2	82.42 ± 0.43
SAM 3a	66.59 ± 1.66
SAM 3b	82.53 ± 0.41

dx.doi.org/10.1021/am500049q | *ACS Appl. Mater. Interfaces* 2014, 6, 3712−3720

contact angles for the self-assembled monolayers studied. The higher contact angles that the monolayers exhibit relative to those of a clean gold substrate suggests the formation of a more hydrophobic surface as expected (see Figure S13, Supporting Information). The higher contact angle of **SAM 1** (97°) compared to **SAM 2** (82°) and **3b** (83°) can be explained by different molecular orientations of the films. In **SAM 1**, the presence of S−Au interactions orients the molecules in such a way that the fullerene and TPA moieties are exposed to the liquid−solid interface. The contact angle of this monolayer is comparable to those reported by Honciuc et al. for TPA-based fullerene compounds (Θ = 93° and 76° for fullerene and triphenylamine exposed moieties to the liquid−solid interface, respectively).[42] Additionally, the formation of **SAM 3b** was evidenced by the difference in contact angles between **SAM 3a** and **3b**. **SAM 3a** exhibits a lower contact angle as expected for an amine-terminated monolayer that can undergo hydrogen bonding with water, therefore, increasing wettability. The **SAM 3b** contact angle is comparable to those of **SAM 1** and **SAM 2** which possess fullerene-based monolayers.

All SAMs were probed for their passivating ability toward $Fe(CN)_6^{3-/4-}$ and $Ru(NH_3)_6^{2+/3+}$ as shown in Figures S14 and S15, Supporting Information. An unmodified gold electrode was also studied as a control which shows reversible behavior for the $Fe(CN)_6^{3-/4-}$ and $Ru(NH_3)_6^{2+/3+}$ redox couples. In all cases, there is an almost quantitative suppression of the observed currents of the two electroactive probe ions, but **SAM 3a** is less effective than the other monolayers in blocking the electroactivity of the probes, see Figures S15b and S16b, Supporting Information. This could be due to a less densely packed SAM in the case of **SAM 3a** or to a more effective electron transfer across the SAM.

To quantify the surface coverage by the fullerene-based dyads, quartz crystal microbalance (QCM) measurements were performed to detect the small mass changes that occur at the surface as a function of time. The QCM profiles of **SAM 1**−**3** show that no frequency change is observed in pure toluene at 25 °C, and after the addition of aminothiophenol or the dyad solution, the resonant frequencies decrease (Figure 3). The changes in frequency correspond to the adsorption of 1.18×10^{-10}, 0.82×10^{-10}, and 2.7×10^{-10} for **SAM 1**, **2**, and **3a**, respectively. These values are relatively close to reported values for related compounds, 2.0×10^{-10} mol/cm^2 for C_{60},[43] 1.6×10^{-10} mol/cm^2 for ferrocene−C_{60},[33] and 7.4×10^{-10} mol/cm^2 for alkanethiol.[44] *cis*-**1** shows better coverage for Au than the other monolayers.

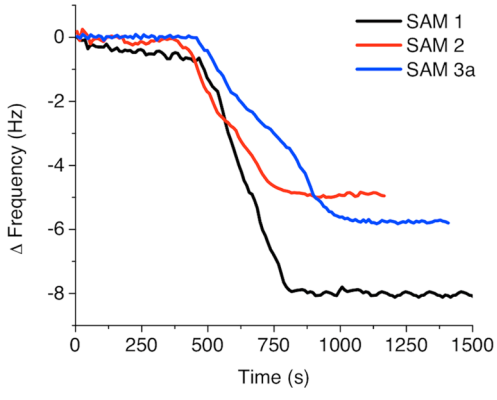

Figure 3. Resonance frequency changes of Au quartz crystal during the formation of the SAMs.

The fact that the TPA−C_{60} dyad with the thiol group, *cis*-**1**, shows better packing than 4-aminothiophenol could be related to the attraction between the fullerenes, which helps the formation of a more densely packed film, compared to the simple 4-aminothiophenol compound. QCM, CV, and contact angle measurements confirm the formation of SAMs on the Au surface. However, these techniques do not provide information about the binding of the SAM to the Au surface. Many groups have studied the formation of thiol-based SAMs of fullerenes or fullerene derivatives on various substrates, particularly on Au surfaces, but little attention has been paid to the C_{60}−C_{60} or Au−C_{60} interaction, which can be in competition with Au−S interaction.[21,32,33,36,43] The X-ray photoelectron (XPS) study of Shirai et al. with thiol-based SAMs of fullerenes shows that, since the Au−S bond strength is similar to that of the fullerene on gold, and also because of the tendency of fullerenes to form clusters, some thiol groups may not bind to the gold surface.[45]

Electrochemical desorption of the thiol groups in KOH solutions was also used to evaluate the surface coverage of the SAMs.[46] Electrochemical desorption experiments were performed using 0.5 M KOH for **SAM 1** and **3a**. The SAM-modified gold electrodes were immersed into a thoroughly Ar degassed KOH solution for 25 min. Cathodic sweeps of the modified gold electrodes between −0.2 and −1.35 V using a scan rate of 100 mV/s exhibit an irreversible wave around −0.9 V (Figure 4). This peak is attributed to the desorption of the

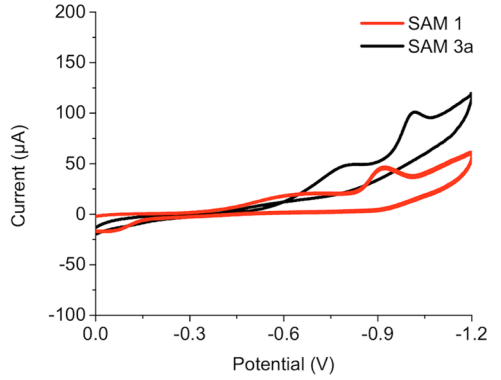

Figure 4. Electrochemical desorption of **SAM 1** and **3a** on Au in 0.5 M KOH solution.

surface-attached thiolates. A similar shape and position of the desorption peak was reported previously for thioctic acid and thiolates.[46−48] Integration of the current under the desorption peak leads to values of 1.9×10^{-10} and 3.8×10^{-10} mol/cm^2 for **SAM 1** and **3a**, respectively, which are in agreement with the values obtained from the QCM measurements. However, there is a slight difference between the QCM results and those from KOH desorption measurement values. These small differences could reflect the adsorption lengths, which are very different for both experiments. The elapsed times in the QCM experiments are significantly short (minutes) when compared to the time for SAMs formed on Au/Cr substrates (hours). After SAM removal, CV measurements showed reversible behavior for the probe ions, thus confirming the quantitative removal of the monolayers.

The resistance to charge transfer of the SAM-modified Au surfaces was also probed using electrochemical impedance

spectroscopy in the presence of $Fe(CN)_6^{3-/4-}$ and $Ru(NH_3)_6^{2+/3+}$. Electrochemical impedance is useful to determine resistances, capacities, and diffusion contributions. The impedance Nyquist plots for all Au modified SAMs are presented in Figure 5. All curves exhibit a semicircular loop in

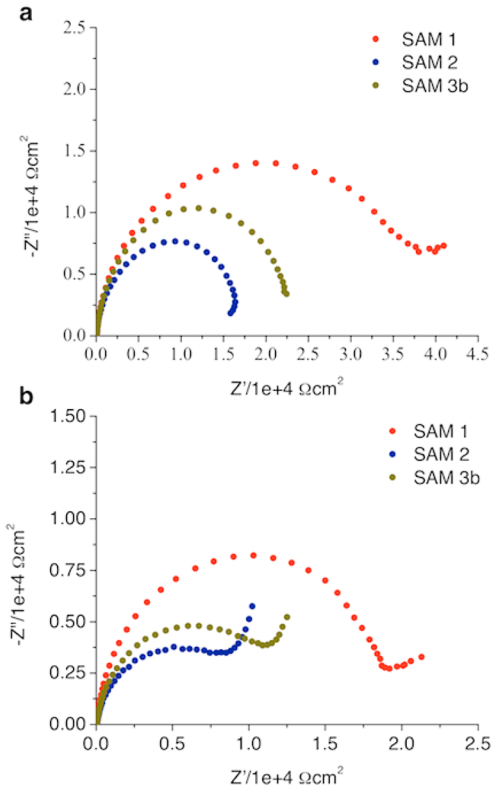

Figure 5. Impedance responses of (a) $Fe(CN)_6^{3-/4-}$ and (b) $Ru(NH_3)_6^{2+/3+}$ for **SAM 1**, **2**, and **3b**.

the high-frequency region, followed by a linear portion at low frequencies, indicating diffusion processes for some of the monolayers. The charge-transfer process between the electrode and the charged redox couple in solution can be analyzed using the equivalent circuit model that reflects the real electrochemical processes using a fitting procedure (Figure 6).

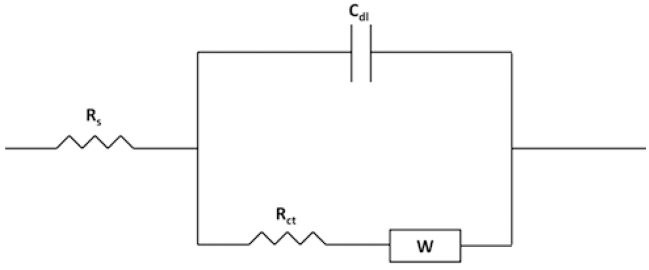

Figure 6. Designed equivalent circuit.

The equivalent circuit was fitted with Randal's model, which includes an ohmic solution resistance between the SAM-modified Au electrode and the reference electrode, R_s, in series with a circuit representing the SAM/solution interface. This circuit consists of a charge-transfer resistance between the SAM and the solution, R_{ct}, which is in parallel with a constant phase element, CPE, and in series with a Warburg diffusion element, W, typically resulting from solution redox species penetrating through pinholes or from defects present in the monolayer. The CPE might be associated with the double layer capacitance at the interface between the SAM and the electrolyte solution. Table 2 presents the equivalent circuit element values obtained

Table 2. Charge-Transfer Resistance of $Fe(CN)_6^{3-/4-}$ and $Ru(NH_3)_6^{2+/3+}$ on SAM 1, 2, and 3b in the presence/absence of UV Illumination

	R_{ct} (Ω cm^2) for $Fe(CN)_6^{3-/4-}$		R_{ct} (Ω cm^2) for $Ru(NH_3)_6^{2+/3+}$	
	no UV light	UV light	no UV light	UV light
SAM 1	3.8×10^4	2.6×10^4	1.9×10^4	2.5×10^4
SAM 2	1.6×10^4	1.4×10^4	0.8×10^4	1.1×10^4
SAM 3b	2.2×10^4	1.6×10^4	1.1×10^4	1.3×10^4

by fitting the experimental values for unmodified and modified gold surfaces with different SAMs in the presence of $Fe(CN)_6^{3-/4-}$ and $Ru(NH_3)_6^{2+/3+}$.

The modification results in an increase in charge-transfer resistance (R_{CT}) for $Fe(CN)_6^{3-/4-}$ from 0.55 Ω cm^2, for the unmodified gold, to 3.8×10^4, 1.6×10^4, and 2.2×10^4 Ω cm^2 for **SAM 1**, **2**, and **3b**, respectively. On the other hand, the R_{CT} for $Ru(NH_3)_6^{2+/3+}$ increases from 0.33 Ω cm^2 to 1.9×10^4, 0.8×10^4, and 1.3×10^4 Ω cm^2 for **SAM 1**, **2**, and **3b**, respectively (Table 2). **SAM 1** exhibits the largest charge-transfer resistance, likely indicating a better packed monolayer for this compound, confirming the QCM results. The charge-transfer resistance for $Fe(CN)_6^{3-/4-}$ and $Ru(NH_3)_6^{2+/3+}$ decreases in the order: **SAM 1** > **SAM 3b** > **SAM 2**. This was the anticipated result in view of the fact that no S−Au interactions exist for **SAM 2** and **SAM 1** possesses well-defined thiol containing molecular structures that do not rely on noncontrolled interfacial reactions as for **SAM 3b**. The equivalent circuit fitting analysis for all impedance plots showed that $Ru(NH_3)_6^{2+/3+}$ always exhibits lower charge-transfer resistances and larger Warburg impedances than $Fe(CN)_6^{3-/4-}$. Similar behavior has been previously observed and ascribed to different factors such as fast homogeneous electron self-exchange kinetics for $Ru(NH_3)_6^{2+/3+}$, which can lead to relatively rapid interfacial electron-transfer kinetics at a SAM-modified electrode.[49] It has also been reported that the slower electron-transfer rate in the case of $Fe(CN)_6^{3-/4-}$ is due to the higher charge.[48] Alternatively, Ganesh and Lakshminarayanan explained these differences between the probe ions invoking a tunneling effect for $Ru(NH_3)_6^{2+/3+}$. Blumberger and Sprik reported that the electron-transfer reaction for $Ru(NH_3)_6^{2+/3+}$ is an outer sphere reaction in which the redox species exchanges electron through a bridge without penetrating the layer.[50]

After establishing the impedance behavior of the different SAMs, we performed similar experiments in the presence of UV irradiation. We monitored the same electrodes in the presence of UV light using both $Fe(CN)_6^{3-/4-}$ and $Ru(NH_3)_6^{2+/3+}$ as electrochemical probes. The impedance responses for **SAM 1**, **2**, and **3b** in the presence and absence of UV light are presented in Figures 7, 8, and 9 (Figures S16−S21, Supporting Information).

Upon illumination, the electrode surfaces showed a significant decrease in the value of R_{ct} for all SAMs in the presence of $Fe(CN)_6^{3-/4-}$ and a corresponding increase for $Ru(NH_3)_6^{2+/3+}$ (Table 2). These results clearly indicate the development of positive charge on the surfaces upon UV irradiation. The increases in R_{CT} in the case of $Ru(NH_3)_6^{2+/3+}$

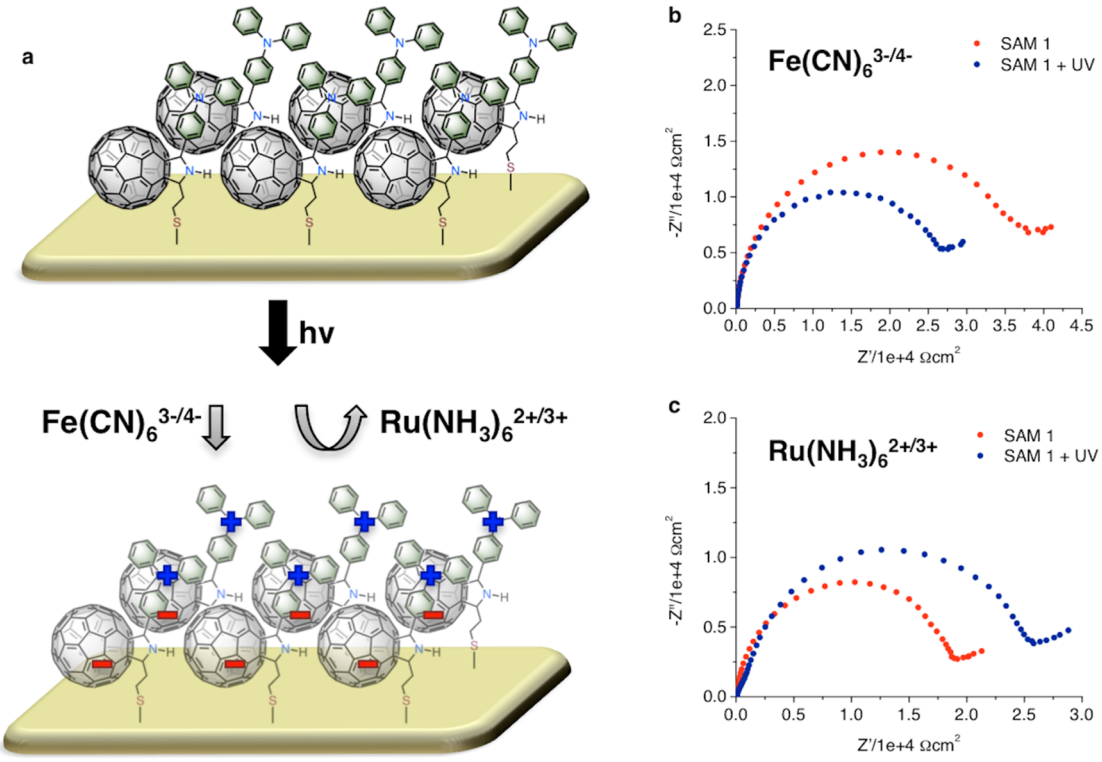

Figure 7. (a) Pictorial representation of **SAM 1** before and after UV-light irradiation and impedance response in the absence/presence of UV light for the charged probes (b) $Fe(CN)_6^{3-/4-}$ and (c) $Ru(NH_3)_6^{2+/3+}$.

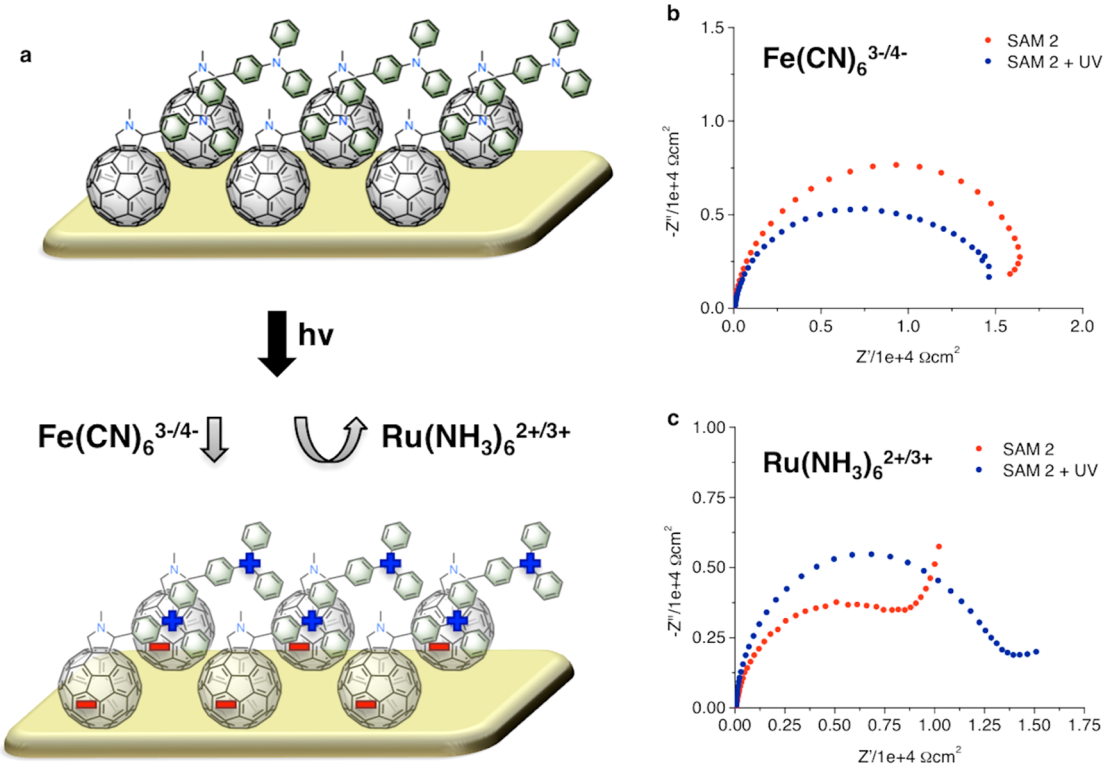

Figure 8. (a) Pictorial representation of **SAM 2** before and after UV-light irradiation and impedance response in the absence/presence of UV light for the charged probes (b) $Fe(CN)_6^{3-/4-}$ and (c) $Ru(NH_3)_6^{2+/3+}$.

result from the electrostatic repulsion between the positively charged probe and the positively charged SAM surface (Figures 7a–9a). In the same way, the electrostatic attraction between the negatively charged probe $Fe(CN)_6^{3-/4-}$ and the positively charged SAM surface results in a higher local concentration of the redox probe that facilitates electron transfer. This phenomenon results from the photoinduced intramolecular charge-transfer processes for these dyads (D^+–A^-). Upon

dx.doi.org/10.1021/am500049q | ACS Appl. Mater. Interfaces 2014, 6, 3712–3720

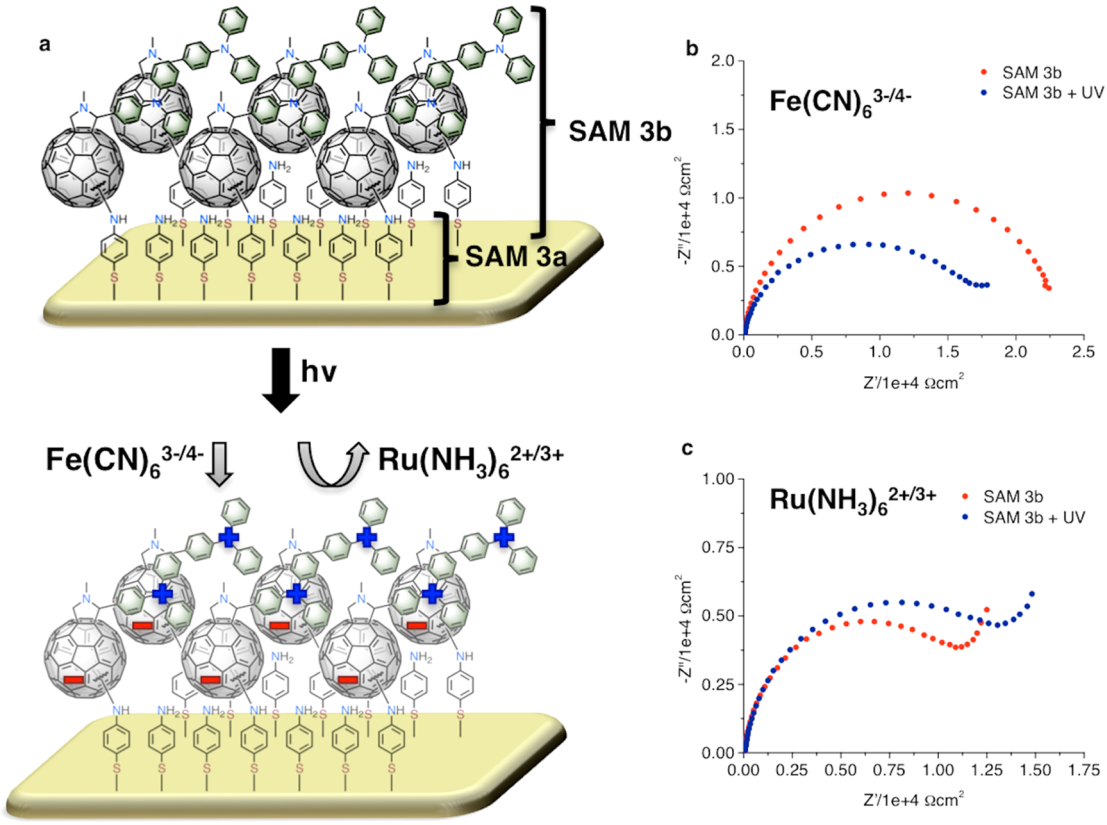

Figure 9. (a) Pictorial representation of **SAM 3b** before and after UV-light irradiation and impedance response in the absence/presence of UV light for the charged probes (b) $Fe(CN)_6^{3-/4-}$ and (c) $Ru(NH_3)_6^{2+/3+}$.

photoexcitation, intramolecular electron transfer from the donor, TPA, to the acceptor, C_{60}, yields the charge-separated states. Although it is possible to oxidize thiol groups in the presence of UV illumination,[51] in our case, no such processes were observed since KOH desorption was performed after the UV irradiation experiments for **SAM 1** and **3b**, and the values are in agreement with those performed by the QCM measurements.

4. CONCLUSION

In this work, we described a simple one step synthesis of a thiol functionalized TPA–C_{60} dyad. Three SAMs of TPA–C_{60} compounds with different anchors were prepared on Au surfaces, and their electrochemical and charge separation properties were investigated using CV, QCM, and electrochemical impedance spectroscopy. Contact angle and electrochemical impedance measurements in the presence of both negative and positive ion probes show that all SAMs form a relatively well packed film on the Au surfaces. Although **SAM 1** is likely a mixture of enantiomers, it was the most densely packed. In future work, it would be interesting to prepare enantiomerically pure fullerene-based self-assembled monolayers and study their packing characteristics as well as their effect on charge separation efficiencies upon irradiation. Although triphenylamines are known to have limited light absorptivity, mainly in the UV region of the spectrum, the impedance response of $Fe(CN)_6^{3-/4-}$ and $Ru(NH_3)_6^{2+/3+}$ in the presence and absence of UV light clearly show that light absorption was sufficient to generate polarized SAMs with positively charged surfaces. We are currently working with porphyrin-fullerene dyad SAMs with higher light absorptivity on transparent conductive oxide electrodes in order to increase the efficiencies and charge polarization. Given that these SAMs absorb a minimal amount of the solar radiation, no adverse effects on the absorption by the photoactive layers are anticipated.

■ ASSOCIATED CONTENT

Supporting Information

^1H NMR, ^{13}C NMR, COSY, NOESY, MALDI-TOF MS, UV–vis, and CV of *trans*-**1** and *cis*-**1**. EIS data for **SAM 1**, **2**, and **3b**. Contact angle images before and after monolayer treatments. This material is available free of charge via the Internet at http://pubs.acs.org.

■ AUTHOR INFORMATION

Corresponding Author

*E-mail: echegoyen@utep.edu.

Author Contributions

‡M.H. and D.M.R.-N. contributed equally. The manuscript was written from contributions of all authors. All authors have given approval to the final version of the manuscript.

Notes

The authors declare no competing financial interest.

■ ACKNOWLEDGMENTS

The authors wish to thank the US Air Force Office of Scientific Research (Grants FA9550-12-1-0053 and FA9550-12-1-0468) and the Robert A. Welch Foundation (Grant No. AH-0033) for generous support for this work. The authors also thank Ping Peng for technical advice.

REFERENCES

(1) Manceau, M.; Angmo, D.; Jørgensen, M.; Krebs, F. C. ITO-free Flexible Polymer Solar Cells: From Small Model Devices to Roll-to-Roll Processed Large Modules. *Org. Electron.* **2011**, *12*, 566−574.

(2) Krebs, F. C. Fabrication and Processing of Polymer Solar Cells: A Review of Printing and Coating Techniques. *Sol. Energy Mater. Sol. Cells* **2009**, *93*, 394−412.

(3) Ghasemi Varnamkhasti, M.; Fallah, H. R.; Mostajaboddavati, M.; Ghasemi, R.; Hassanzadeh, A. Comparison of Metal Oxides as Anode Buffer Layer for Small Molecule Organic Photovoltaic Cells. *Sol. Energy Mater. Sol. Cells* **2012**, *98*, 379−384.

(4) Lim, J. T.; Lee, J. H.; Park, J. K.; Park, B. J.; Yeom, G. Y. Top-emitting Organic Light-emitting Diodes Based on Semitransparent Conducting Cathode of Ba/Al/ITO. *Surf. Coat. Technol.* **2008**, *202*, 5646−5649.

(5) Moliton, A.; Nunzi, J.-M. How to Model the Behaviour of Organic Photovoltaic Cells. *Polym. Int.* **2006**, *55*, 583−600.

(6) Pivrikas, A.; Sariciftci, N. S.; Juška, G.; Österbacka, R. A Review of Charge Transport and Recombination in Polymer/Fullerene Organic Solar Cells. *Prog. Photovoltaics: Res. Appl.* **2007**, *15*, 677−696.

(7) Irwin, M. D.; Liu, J.; Leever, B. J.; Servaites, J. D.; Hersam, M. C.; Durstock, M. F.; Marks, T. J. Consequences of Anode Interfacial Layer Deletion. HCl-Treated ITO in P3HT:PCBM-Based Bulk-Heterojunction Organic Photovoltaic Devices. *Langmuir* **2009**, *26*, 2584−2591.

(8) Hains, A. W.; Liu, J.; Martinson, A. B. F.; Irwin, M. D.; Marks, T. J. Anode Interfacial Tuning via Electron-Blocking/Hole-Transport Layers and Indium Tin Oxide Surface Treatment in Bulk-Heterojunction Organic Photovoltaic Cells. *Adv. Funct. Mater.* **2010**, *20*, 595−606.

(9) Hains, A. W.; Ramanan, C.; Irwin, M. D.; Liu, J.; Wasielewski, M. R.; Marks, T. J. Designed Bithiophene-Based Interfacial Layer for High-Efficiency Bulk-Heterojunction Organic Photovoltaic Cells. Importance of Interfacial Energy Level Matching. *ACS Appl. Mater. Interfaces* **2009**, *2*, 175−185.

(10) Wang, F.; Xiong, T.; Qiao, X.; Ma, D. Origin of Improvement in Device Performance via the Modification Role of Cesium Hydroxide Doped tris(8-hydroxyquinoline) Aluminum Interfacial Layer on ITO Cathode in Inverted Bottom-Emission Organic Light-Emitting Diodes. *Org. Electron.* **2009**, *10*, 266−274.

(11) Khalifa, M. B.; Vaufrey, D.; Bouazizi, A.; Tardy, J.; Maaref, H. Hole Injection and Transport in ITO/PEDOT/PVK/Al Diodes. *Mater. Sci. Eng., C* **2002**, *21*, 277−282.

(12) Jørgensen, M.; Norrman, K.; Krebs, F. C. Stability/Degradation of Polymer Solar Cells. *Sol. Energy Mater. Sol. Cells* **2008**, *92*, 686−714.

(13) Kemerink, M.; Timpanaro, S.; de Kok, M. M.; Meulenkamp, E. A.; Touwslager, F. J. Three-Dimensional Inhomogeneities in PEDOT:PSS Films. *J. Phys. Chem. B* **2004**, *108*, 18820−18825.

(14) Lee, J.; Jung, B.-J.; Lee, J.-I.; Chu, H. Y.; Do, L.-M.; Shim, H.-K. Modification of an ITO Anode with a Hole-transporting SAM for Improved OLED Device Characteristics. *J. Mater. Chem.* **2002**, *12*, 3494−3498.

(15) Chong, L.-W.; Lee, Y.-L.; Wen, T.-C. Surface Modification of Indium Tin Oxide Anodes by Self-assembly Monolayers: Effects on Interfacial Morphology and Charge Injection in Organic Light-emitting Diodes. *Thin Solid Films* **2007**, *515*, 2833−2841.

(16) Besbes, S.; Ouada, H. B.; Davenas, J.; Ponsonnet, L.; Jaffrezic, N.; Alcouffe, P. Effect of Surface Treatment and Functionalization on the ITO Properties for OLEDs. *Mater. Sci. Eng., C* **2006**, *26*, 505−510.

(17) Beaumont, N.; Hancox, I.; Sullivan, P.; Hatton, R. A.; Jones, T. S. Increased Efficiency in Small Molecule Organic Photovoltaic Cells through Electrode Modification with Self-assembled Monolayers. *Energy Environ. Sci.* **2011**, *4*, 1708−1711.

(18) Araki, Y.; Ito, O. Factors Controlling Lifetimes of Photoinduced Charge-Separated States of Fullerene-Donor Molecular Systems. *J. Photochem. Photobiol., C: Photochem. Rev.* **2008**, *9*, 93−110.

(19) González-Rodríguez, D.; Torres, T.; Herranz, M. Á.; Echegoyen, L.; Carbonell, E.; Guldi, D. M. Screening Electronic Communication through *ortho*-, *meta*- and *para*-Substituted Linkers Separating Subphthalocyanines and C_{60}. *Chem.—Eur. J.* **2008**, *14*, 7670−7679.

(20) Imahori, H.; Hagiwara, K.; Aoki, M.; Akiyama, T.; Taniguchi, S.; Okada, T.; Shirakawa, M.; Sakata, Y. Linkage and Solvent Dependence of Photoinduced Electron Transfer in Zincporphyrin-C_{60} Dyads. *J. Am. Chem. Soc.* **1996**, *118*, 11771−11782.

(21) D'Souza, F.; Deviprasad, G. R.; El-Khouly, M. E.; Fujitsuka, M.; Ito, O. Probing the Donor−Acceptor Proximity on the Physicochemical Properties of Porphyrin−Fullerene Dyads: "Tail-On" and "Tail-Off" Binding Approach. *J. Am. Chem. Soc.* **2001**, *123*, 5277−5284.

(22) Guldi, D. M.; Hirsch, A.; Scheloske, M.; Dietel, E.; Troisi, A.; Zerbetto, F.; Prato, M. Modulating Charge-Transfer Interactions in Topologically Different Porphyrin−C_{60} Dyads. *Chem.—Eur. J.* **2003**, *9*, 4968−4979.

(23) Guldi, D. M.; Luo, C.; Prato, M.; Troisi, A.; Zerbetto, F.; Scheloske, M.; Dietel, E.; Bauer, W.; Hirsch, A. Parallel (Face-to-Face) Versus Perpendicular (Edge-to-Face) Alignment of Electron Donors and Acceptors in Fullerene Porphyrin Dyads: The Importance of Orientation in Electron Transfer. *J. Am. Chem. Soc.* **2001**, *123*, 9166−9167.

(24) Fazio, M. A.; Durandin, A.; Tkachenko, N. V.; Niemi, M.; Lemmetyinen, H.; Schuster, D. I. Synthesis, Conformational Interconversion, and Photophysics of Tethered Porphyrin−Fullerene Dyads with Parachute Topology. *Chem.—Eur. J.* **2009**, *15*, 7698−7705.

(25) Sandanayaka, A. S. D.; Sasabe, H.; Araki, Y.; Furusho, Y.; Ito, O.; Takata, T. Photoinduced Electron-Transfer Processes between [60]Fullerene and Triphenylamine Moieties Tethered by Rotaxane Structures. Through-Space Electron Transfer via Excited Triplet States of [60]Fullerene. *J. Phys. Chem. A* **2004**, *108*, 5145−5155.

(26) Jousselme, B.; Blanchard, P.; Levillain, E.; de Bettignies, R.; Roncali, J. Electrochemical Synthesis of C_{60}-Derivatized Poly(thiophene)s from Tailored Precursors. *Macromolecules* **2003**, *36*, 3020−3025.

(27) Handa, S.; Giacalone, F.; Haque, S. A.; Palomares, E.; Martín, N.; Durrant, J. R. Solid Film versus Solution-Phase Charge-Recombination Dynamics of exTTF−Bridge−C_{60} Dyads. *Chem.—Eur. J.* **2005**, *11*, 7440−7447.

(28) Poddutoori, P. K.; Sandanayaka, A. S. D.; Hasobe, T.; Ito, O.; van der Est, A. Photoinduced Charge Separation in a Ferrocene−Aluminum(III) Porphyrin−Fullerene Supramolecular Triad. *J. Phys. Chem. B* **2010**, *114*, 14348−14357.

(29) El-Khouly, M. E.; Kim, J. H.; Kwak, M.; Choi, C. S.; Ito, O.; Kay, K.-Y. Photoinduced Charge Separation of the Covalently Linked Fullerene-Triphenylamine-Fullerene Triad. Effect of Dual Fullerenes on Lifetimes of Charge-Separated States. *Bull. Chem. Soc. Jpn.* **2007**, *80*, 2465−2472.

(30) Zalesny, R.; Loboda, O.; Iliopoulos, K.; Chatzikyriakos, G.; Couris, S.; Rotas, G.; Tagmatarchis, N.; Avramopoulos, A.; Papadopoulos, M. G. Linear and Nonlinear Optical Properties of Triphenylamine-functionalized C_{60}: Insights from Theory and Experiment. *Phys. Chem. Chem. Phys.* **2010**, *12*, 373−381.

(31) Maggini, M.; Scorrano, G.; Prato, M. Addition of Azomethine Ylides to C_{60}: Synthesis, Characterization, and Functionalization of Fullerene Pyrrolidines. *J. Am. Chem. Soc.* **1993**, *115*, 9798−9799.

(32) Pinzón, J. R.; Gasca, D. C.; Sankaranarayanan, S. G.; Bottari, G.; Torres, T. s.; Guldi, D. M.; Echegoyen, L. Photoinduced Charge Transfer and Electrochemical Properties of Triphenylamine I_h-Sc_3N@C_{80} Donor−Acceptor Conjugates. *J. Am. Chem. Soc.* **2009**, *131*, 7727−7734.

(33) Hoang, V. T.; Rogers, L. M.; D'Souza, F. Synthesis and Formation of Monolayer Self-assembly of Thiol Appended Fullerenes and Fullerene−ferrocene Dyads on Gold Electrode. *Electrochem. Commun.* **2002**, *4*, 50−53.

(34) Kira, A.; Umeyama, T.; Matano, Y.; Yoshida, K.; Isoda, S.; Park, J. K.; Kim, D.; Imahori, H. Supramolecular Donor/Acceptor Heterojunctions by Vectorial Stepwise Assembly of Porphyrins and Coordination-Bonded Fullerene Arrays for Photocurrent Generation. *J. Am. Chem. Soc.* **2009**, *131*, 3198−3200.

(35) Ranta, J.; Kaunisto, K.; Niskanen, M.; Efimov, A.; Hukka, T. I.; Lemmetyinen, H. Monoisomeric Phthalocyanines and Phthalocyanine-Fullerene Dyads with Polar Side Chains: Synthesis, Modeling, and Photovoltage. *J. Phys. Chem. C* **2014**, DOI: 10.1021/jp4096002.
(36) Shi, X.; Caldwell, W. B.; Chen, K.; Mirkin, C. A. A Well-Defined Surface-Confinable Fullerene: Monolayer Self-assembly on Au(111). *J. Am. Chem. Soc.* **1994**, *116*, 11598−11599.
(37) Sahoo, R. R.; Patnaik, A. Surface Confined Self-assembled Fullerene Nanoclusters: A Microscopic Study. *Appl. Surf. Sci.* **2005**, *245*, 26−38.
(38) Lukoyanova, O.; Cardona, C. M.; Altable, M.; Filippone, S.; Martín Domenech, Á.; Martín, N.; Echegoyen, L. Selective Electrochemical Retro-Cycloaddition Reaction of Pyrrolidinofullerenes. *Angew. Chem., Int. Ed.* **2006**, *45*, 7430−7433.
(39) Han, H.; Tachikawa, H. Electrochemical Determination of Thiols at Single-wall Carbon Nanotubes and PPQ Modifed Electrodes. *Front. Biosci.* **2005**, *10*, 931−939.
(40) Tan, W. T.; Bond, A. M.; Ngooi, S. W.; Lim, E. B.; Goh, J. K. Electrochemical Oxidation of L-cysteine Mediated by a Fullerene-C_{60}-modified Carbon Electrode. *Anal. Chim. Acta* **2003**, *491*, 181−191.
(41) Whitesides, G. M.; Laibinis, P. E. Wet Chemical Approaches to the Characterization of Organic Surfaces: Self-assembled Monolayers, Wetting, and the Physical-Organic Chemistry of the Solid-Liquid Interface. *Langmuir* **1990**, *6*, 87−96.
(42) Honciuc, A.; Jaiswal, A.; Gong, A.; Ashworth, K.; Spangler, C. W.; Peterson, I. R.; Dalton, L. R.; Metzger, R. M. Current Rectification in a Langmuir-Schaefer Monolayer of Fullerene-*bis*-[4-diphenylamino-4″-(N-ethyl-N-2″-ethyl)amino-1,4-diphenyl-1,3-butadiene] Malonate between Au Electrodes. *J. Phys. Chem. B* **2004**, *109*, 857−871.
(43) Caldwell, W. B.; Chen, K.; Mirkin, C. A.; Babinec, S. J. Self-assembled Monolayer Films of Fullerene C_{60} on Cysteamine-modified Gold. *Langmuir* **1993**, *9*, 1945−1947.
(44) Love, J. C.; Estroff, L. A.; Kriebel, J. K.; Nuzzo, R. G.; Whitesides, G. M. Self-Assembled Monolayers of Thiolates on Metals as a Form of Nanotechnology. *Chem. Rev.* **2005**, *105*, 1103−1170.
(45) Shirai, Y.; Cheng, L.; Chen, B.; Tour, J. M. Characterization of Self-Assembled Monolayers of Fullerene Derivatives on Gold Surfaces: Implications for Device Evaluations. *J. Am. Chem. Soc.* **2006**, *128*, 13479−13489.
(46) Wang, Y.; Kaifer, A. E. Interfacial Molecular Recognition. Binding of Ferrocenecarboxylate to *β*-Aminocyclodextrin Hosts Electrostatically Immobilized on a Thioctic Acid Monolayer. *J. Phys. Chem. B* **1998**, *102*, 9922−9927.
(47) Dong, Y.; Abaci, S.; Shannon, C.; Bozack, M. J. Self-Assembly and Electrochemical Desorption of Thioctic Acid Monolayers on Gold Surfaces. *Langmuir* **2003**, *19*, 8922−8926.
(48) Zhang, S.; Echegoyen, L. Selective Anion Sensing by a Tris-Amide CTV Derivative: ^{1}H NMR Titration, Self-Assembled Monolayers, and Impedance Spectroscopy. *J. Am. Chem. Soc.* **2005**, *127*, 2006−2011.
(49) Groat, K. A.; Creager, S. E. Self-assembled Monolayers in Organic Solvents: Electrochemistry at Alkanethiolate-coated Gold in Propylene Carbonate. *Langmuir* **1993**, *9*, 3668−3675.
(50) Blumberger, J.; Sprik, M. Ab Initio Molecular Dynamics Simulation of the Aqueous Ru^{2+}/Ru^{3+} Redox Reaction: The Marcus Perspective. *J. Phys. Chem. B* **2005**, *109*, 6793−6804.
(51) Huang, J.; Hemminger, J. C. Photooxidation of Thiols in Self-assembled Monolayers on Gold. *J. Am. Chem. Soc.* **1993**, *115*, 3342−3343.